Journal of Biomedical Optics

BiomedicalOptics.SPIEDigitalLibrary.org

Accurate extraction of optical properties and top layer thickness of two-layered mucosal tissue phantoms from spatially resolved reflectance spectra

Kung-Bin Sung
Kuang-Wei Shih
Fang-Wei Hsu
Hong-Po Hsieh
Min-Jie Chuang
Yi-Hsien Hsiao
Yu-Hui Su
Gen-Hao Tien

SPIE.

Accurate extraction of optical properties and top layer thickness of two-layered mucosal tissue phantoms from spatially resolved reflectance spectra

Kung-Bin Sung,[a,b,c,*] Kuang-Wei Shih,[a] Fang-Wei Hsu,[a] Hong-Po Hsieh,[a] Min-Jie Chuang,[a] Yi-Hsien Hsiao,[a] Yu-Hui Su,[a] and Gen-Hao Tien[a]
[a]National Taiwan University, Graduate Institute of Biomedical Electronics and Bioinformatics, No. 1 Sec. 4 Roosevelt Road, Taipei 10617, Taiwan
[b]National Taiwan University, Department of Electrical Engineering, No. 1 Sec. 4 Roosevelt Road, Taipei 10617, Taiwan
[c]National Taiwan University, Molecular Imaging Center, No. 1 Sec. 4 Roosevelt Road, Taipei 10617, Taiwan

Abstract. We are reporting on an experimental investigation of a movable diffuse reflectance spectroscopy system to extract diagnostically relevant optical properties of two-layered tissue phantoms simulating mucosae that are covered with stratified squamous epithelium. The reflectance spectra were measured at multiple source-detector separations using two imaging fiber bundles in contact with the phantoms, one with its optical axis perpendicular to the sample surface (perpendicular probe) and the other with its distal end beveled and optical axis tilted at 45 deg (oblique probe). Polystyrene microspheres and purified human hemoglobin were used to make tissue phantoms whose scattering and absorption properties could be well controlled and theoretically predicted. Monte Carlo simulations were used to predict the reflectance spectra for system calibration and an iterative curve fitting that simultaneously extracted the top layer reduced scattering coefficient, thickness, bottom layer reduced scattering coefficient, and hemoglobin concentration of the phantoms. The errors of the recovered parameters ranged from 7% to 20%. The oblique probe showed higher accuracy in the extracted top layer reduced scattering coefficient and thickness than the perpendicular probe. The developed system and data analysis methods provide a feasible tool to quantify the optical properties *in vivo*. [DOI: 10.1117/1.JBO.19.7.077002]

Keywords: diffuse reflectance spectroscopy; Monte Carlo; optical properties; stratified squamous epithelium; dysplasia.

Paper 140191R received Mar. 20, 2014; revised manuscript received Jun. 13, 2014; accepted for publication Jun. 17, 2014; published online Jul. 15, 2014.

1 Introduction

Diffuse reflectance spectroscopy (DRS) has been applied to obtain diagnostically relevant information of tissue *in vivo* for detecting epithelial dysplasia, which is a precursor of many cancers and has more successful treatments than more advanced malignancies.[1] In many steady-state DRS studies on the stratified squamous epithelium, such as those in the mucosae of the oral cavity, the esophagus and uterine cervix, the mucosal tissue has been modeled as a homogeneous semi-infinite medium. Optical properties, including the reduced scattering coefficient (μ_s') and the absorption coefficient (μ_a) of the homogeneous tissue models are estimated from reflectance measurements using various inverse methods based on the diffusion approximation to the radiative transport equation,[2,3] Monte Carlo simulations,[4] or empirical relations.[5] For example, *in vivo* DRS studies on the cervical or oral mucosa[2–6] have shown increased μ_a in dysplastic tissue compared to normal tissue. It is well accepted that the higher absorption in dysplastic tissue is caused by increased hemoglobin absorption due to angiogenesis that occurs during precancerous transformation. A decrease in extracted μ_s' with the progression of dysplasia has been reported in studies on cervical mucosa[2,4,6] and attributed to the breakdown of collagen fiber networks in the superficial stroma underneath the epithelial layer. Major characteristics of dysplasia in the epithelium include enlarged, irregularly shaped and hyperchromatic cell nuclei, and increased nuclear-to-cytoplasmic ratios. We expect these morphological changes to increase the scattering coefficient (μ_s) of the epithelium.[7–9] Because these diagnostically relevant changes in tissue have confounding effects on the measured reflectance, the ability to quantify the μ_s' of a top epithelial layer and both the μ_s' and μ_a of an underlying stroma are promising to improve the accuracy of DRS to discriminate dysplastic lesions from normal mucosal tissue.

Recent efforts to estimate the μ_s', μ_a, and the thickness of the top layer of two-layered mucosal tissue models from DRS measurements have resulted in limited success.[10–15] The major challenge is to accurately recover the thickness and μ_s' of a thin (about 0.2–0.6 mm) epithelial layer that is highly forward scattering. Liu and Ramanujam proposed a two-step approach in which the epithelial μ_s' and μ_a were extracted from the reflectance detected by angled illumination and collection fibers located at a small source-detector separation (SDS) of 0.3 mm, and the stromal μ_s' and μ_a and the epithelial thickness were extracted from reflectance detected by flat-tipped illumination and collection fibers located at a larger SDS of 1.5 mm.[10] A Monte Carlo-based iterative curve-fitting method was used for extracting the optical properties.[16] Although

*Address all correspondence to: Kung-Bin Sung, E-mail: kbsung@ntu.edu.tw

0091-3286/2014/$25.00 © 2014 SPIE

reasonably high accuracy was obtained for estimating the epithelial μ_s' and thickness from simulated data (errors 10–15%), experimental validation of the proposed probe design has not been reported. Yudovsky and Pilon proposed an empirical model for the skin and demonstrated quite accurate extraction of the concentrations of melanin and hemoglobin, oxygen saturation, and the thickness of the epidermis based on the assumption of identical $\mu_s'(\lambda)$ in both layers.[14]

One strategy to gain depth-resolved information of tissue from reflected photons is using multiple SDSs.[12,13,15,17,18] Wang et al. used a condensed Monte Carlo method to train an artificial neural network for estimating μ_a and μ_s' of two-layered mucosal tissue models and reported errors in the range of 12–34% theoretically and 21–38% experimentally.[12] The method requires *a priori* knowledge of the top layer thickness that limits its application. Yudovsky and Durkin used a similar approach of artificial neural networks trained by Monte Carlo simulations to analyze reflectance resulting from spatially modulated illumination at multiple frequencies.[13] With the restriction of a known and fixed μ_s' in a strongly absorbing top layer, such as the epidermis, this method was shown with simulations to estimate only the optical thickness of the top layer and the μ_s' and μ_a of a semi-infinite bottom layer. Sharma et al. demonstrated moderate accuracy in extracting μ_s' and μ_a of two-layered liquid phantoms and the thickness of the top layer using a Monte Carlo-based iterative curve-fitting approach.[18] The model is limited to samples having identical $\mu_s'(\lambda)$ in both layers. Fredriksson et al. used a Monte Carlo-based skin model to extract the blood fraction and oxygen saturation from the simulated data without noise.[15]

Recently, our group proposed to extract optical properties of two-layered mucosal tissue models by simultaneously analyzing reflectance spectra measured at multiple SDSs while imposing spectral constraints on $\mu_s'(\lambda)$ and $\mu_a(\lambda)$.[17] A theoretical analysis using scalable Monte Carlo simulations showed that the sensitivity to the epithelial μ_s can be enhanced using an oblique fiber optic probe that consists of one source fiber and multiple detection fibers parallel to each other with their optical axes tilted by about 45 deg from the tissue surface normal.[19] Although the previous theoretical investigation achieved high accuracy in extracted epithelial μ_s' (errors about 2%) and other optical properties (errors below 10%), the random Gaussian noise added to simulated spectral data may not fully represent noises in experimental measurements. In addition, correct calibration of the experimental system is crucial to converting measured reflectance data to the true reflectance of a sample and to enabling comparison with model-predicted values for recovery of optical properties. Therefore, here, we report experimental validation of our approach by measuring solid two-layered tissue mimicking phantoms with a movable DRS system and two endoscope-compatible contact probes, one in the conventional perpendicular geometry and the other in the oblique geometry proposed in Ref. 19. Calibration of the nonuniform spectral response of the system was accomplished using aqueous calibration phantoms made of polystyrene microspheres in water for which the μ_s and scattering phase functions were obtained using Mie theory.[20] We made two-layered mucosal tissue phantoms using polystyrene microspheres and purified human hemoglobin, so that the accuracy of recovered optical properties could be quantified by comparison with the expected values based on the concentrations of the materials used. The current study is expected to serve two purposes. The first is to demonstrate the capability of the reported DRS system and data analysis methods to quantify the optical properties of two-layered mucosal tissue phantoms. The second is to provide the first experimental validation of the proposed oblique probe and compare its performance with that of the conventional perpendicular probe geometry. The results will provide information to facilitate the development of spatially resolved DRS methods for improving the noninvasive detection of dysplasia in stratified squamous epithelium.

2 Methods and Materials

2.1 *Spatially Resolved Diffuse Reflectance Spectroscopy System*

Figure 1(a) shows the schematic diagrams of the experimental setup and fiber optic probes to measure spatially resolved reflectance spectra. The whole system was on a utility cart with approximate dimensions of 60 cm (width) × 90 cm (length) × 120 cm (height). Visible light (400–700 nm) from a broadband light source (Bluloop, Ocean Optics, Dunedin, Florida) was focused to a spot with a 350-μm diameter near the center of the proximal end of a coherent imaging fiber bundle (Ming Home CO., Taiwan). The distal end surface of the fiber bundle was intended to be in gentle contact with the surface of a sample under test. Two fiber bundles were used in this study. The distal end of one of the fiber bundles was beveled at 45 deg as illustrated in the inset. Fiber bundles used in this study are 1.5 m long and have about 19,000 optical fibers regularly packed to relay images of reflected light from the sample to the detection part of the system. Individual fibers in the bundles have a core refractive index of 1.61, a core diameter of 15 μm, and a nominal numerical aperture of 0.4. The two fiber bundles were enclosed in Teflon tubes with an outer diameter of 3 mm and sealed at the distal ends to make endoscope-compatible probes. Two linear polarizers oriented orthogonally to each other were used in conjunction with a polarizing beam splitter (PBS) to minimize the specular reflection of the proximal end surface of the fiber bundle. Images of reflected light from a sample were collected by a hyperspectral imaging system (Spectracube, Applied Spectral Imaging, Israel) to acquire a spectrum at each pixel within a wavelength range of 400–700 nm. A circular region covering the illumination spot and its vicinity in the reflected images was blocked by a Cr-coated attenuation plate located at the focal plane of lens L3 (a conjugate plane of the fiber bundle end surfaces) to prevent the saturation of the detector. The effect of the attenuation plate is illustrated in Figs. 1(b) and 1(c), showing images of the proximal ends of the fiber bundles whose distal ends are placed on the surface of a calibration phantom (described in Sec. 2.2). The use of imaging fiber bundles and hyperspectral imaging acquisition enables a flexible selection of regions of interests (ROIs) for spectral analysis in this initial experimental study. For the perpendicular probe that has its optical axis perpendicular to the sample surface, average spectra were obtained from four concentric rings as shown in Fig. 1(b) to exploit the circularly symmetric geometry. The rings are 200-μm wide except for the innermost ring that is 100 μm wide. The center-to-center SDSs between the illumination spot and the detection ROIs are 0.3, 0.4, 0.6, and 0.8 mm. For the oblique probe, the optical axis is tilted by 45 deg from the sample surface normal and the average spectra were calculated from nine circular ROIs at the proximal fiber end as shown in Fig. 1(c). The circular ROIs have a diameter of 200 μm and are located

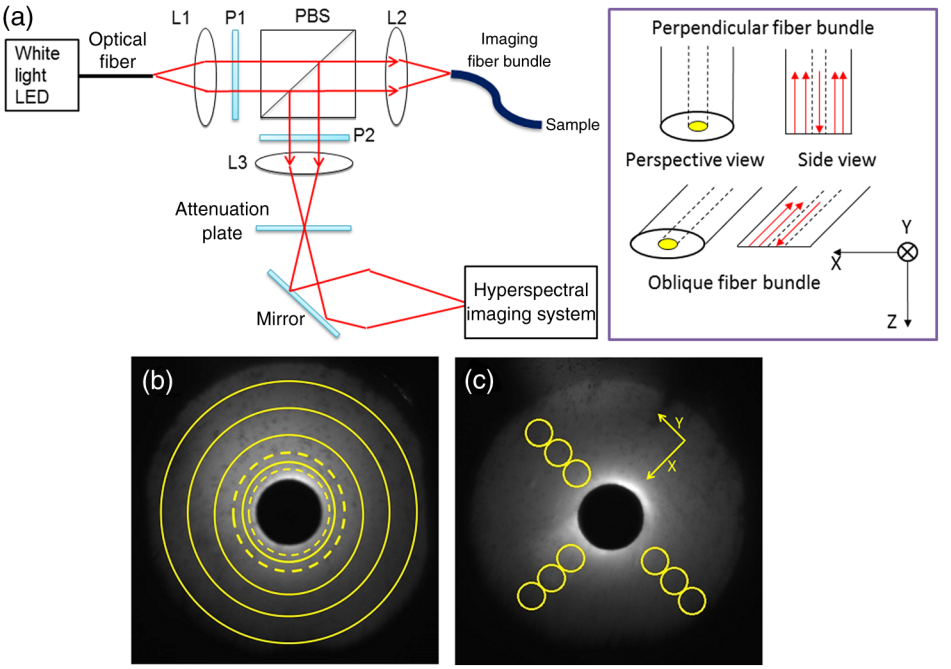

Fig. 1 (a) Schematic diagram of the optical setup. L1, L2, L3: lenses; P1, P2: linear polarizers with crossed orientations; PBS: polarizing beam splitter. The inset illustrates the geometry of the distal ends of two imaging fiber bundles. (b)(c) Reflectance images of the proximal end of the (b) perpendicular and (c) oblique fiber bundle. Yellow lines mark the regions of interest for analysis. To avoid ambiguity, the innermost ring in (b) is shown with dotted lines because it overlaps with the next ring.

at SDSs of 0.4, 0.6, and 0.8 mm, respectively. The three ROIs along the $+y$ axis are mirror images of the three ROIs along the $-y$ axis, and therefore spectra of the ROIs with the same SDS were averaged for subsequent analysis. Note that at the distal end of the oblique fiber bundle, the three ROIs along the x axis have SDSs of 0.57, 0.85, and 1.1 mm due to the 45 deg bevel; the three ROIs along the y axis still have SDSs of 0.4, 0.6, and 0.8 mm. The selection of the ROIs follows the probe design proposed in our previous Monte Carlo study to enhance the sensitivity to the epithelial optical properties.[19]

2.2 *Tissue Phantoms*

Spectral data measured with the movable DRS system are in an arbitrary scale and contain background reflections from optical components in the system. We used a set of four homogeneous aqueous calibration phantoms to establish calibration factors for removing the effects of nonuniform spectral response and background of the system. We chose polystyrene microspheres (Polysciences, Inc., Warrington, Pennsylvania) as the source of scattering over other materials, such as fat emulsions and titanium dioxide powders because the size of polystyrene microspheres can be precisely controlled, which is necessary to accurately predict the μ_s and scattering phase functions. Two of the calibration phantoms contain polystyrene microspheres with a diameter of 0.51 ± 0.008 μm at concentrations of 3.64×10^{10} and 4.85×10^{10} particles/mL, respectively. The other two calibration phantoms contain polystyrene microspheres with a diameter of 0.99 ± 0.03 μm at concentrations of 4.55×10^{9} and 6.07×10^{9} particles/mL, respectively.

To evaluate the performance of recovering optical properties of the two-layered mucosal tissue model, we fabricated six two-layered solid phantoms with the 0.51-μm polystyrene microspheres and human hemoglobin (H0267, Sigma-Aldrich) in 2% agarose gel (Agarose SFR, Amresco). The concentrations of microspheres and hemoglobin used to make the phantoms and the ranges of μ_s' in wavelength range of 450–700 nm are summarized in Table 1. The μ_s' and hemoglobin concentrations of phantoms 1 and 2 were chosen to represent optical properties of normal oral mucosa as reported in previous studies.[21,22] Phantoms 3 to 6 were intended to simulate changes in optical properties associated with dysplasia.[6] No absorption source was added to the top layer because μ_a is at least an order of magnitude smaller than μ_s in the epithelium and has not been found to alter significantly during the development of dysplasia. The thickness of the top layer was controlled by molds made of polydimethylsiloxane (PDMS) on glass slides. Before a slab of solidified agarose gel for making the top layer was laid on the bottom layer, we measured its thickness with a microcaliper. The measured thicknesses are shown in Table 1.

2.3 *Monte Carlo Model*

We implemented a two-layered Monte Carlo model with a compute unified device architect (CUDA, NVIDIA Corporation, Santa Clara, California) to exploit the parallel computing advantage provided by the graphics processing unit (GPU). In the GPU-based Monte Carlo implementation (GPU-MC), two-layered tissue phantoms were modeled as a thin top layer on top of a semi-infinite bottom layer to mimic the structure of stratified squamous epithelial tissue on top of connective tissue. We used variable photon weights and variable step sizes between interaction events to predict the reflectance detected by the predefined ROIs.

The initial position of a photon packet was randomly sampled to have a Gaussian distribution with the e^{-2} diameter

Table 1 Concentrations of polystyrene microspheres ([beads]) and hemoglobin (C_{Hb}) used to make the two-layered phantoms. The top layer thickness (D) measured with a microcaliper and ranges of $\mu_s'(\lambda)$ calculated using Mie theory are also listed.

Phantom number	Top [beads] (#/mL)	Top $\mu_s'(\lambda)$ (cm^{-1})	Bottom [beads] (#/mL)	Bottom $\mu_s'(\lambda)$ (cm^{-1})	C_{Hb} (g/L)	D (mm)
1	3.64×10^{10}	10.5–13.5	7.82×10^{10}	21.0–27.0	1.6	0.36
2	3.64×10^{10}	10.5–13.5	7.82×10^{10}	21.0–27.0	1.6	0.375
3	5.46×10^{10}	13.5–18.5	5.46×10^{10}	13.5–18.5	2.58	0.42
4	5.46×10^{10}	13.5–18.5	5.46×10^{10}	13.5–18.5	2.58	0.39
5	6.37×10^{10}	15.7–21.6	5.46×10^{10}	13.5–18.5	2.58	0.42
6	6.37×10^{10}	15.7–21.6	5.46×10^{10}	13.5–18.5	2.58	0.36

equal to the size of the illumination spot.[23] The initial incident angle of a photon packet was randomly sampled within the range determined by the numerical aperture of the fibers. For the oblique probe, the propagation direction was rotated using a rotation matrix

$$\begin{bmatrix} cx' \\ cy' \\ cz' \end{bmatrix} = \begin{bmatrix} \cos\beta & 0 & \sin\beta \\ 0 & 1 & 0 \\ -\sin\beta & 0 & \cos\beta \end{bmatrix} \begin{bmatrix} cx \\ cy \\ cz \end{bmatrix}, \quad (1)$$

where cx, cy, and cz are direction cosines of the initial propagation direction, and cx', cy', and cz' are direction cosines after rotation.[24] The photon propagation direction was then refracted at the sample surface using Snell's law and refractive indices of the fiber core and water. We set the angle β to be 45 deg during photon launch and −45 deg when a photon packet leaves the sample surface (after refraction at the sample surface). Photon packets leaving the sample within the angular span corresponding to the fiber numerical aperture were deemed to be detected.

In addition to the commonly used Henyey–Greenstein (HG) phase function, the GPU-MC also used wavelength-dependent scattering phase functions of polystyrene microspheres predicted by Mie theory. For each wavelength of interest, a cumulative distribution function of the polar scattering angle between 0 deg and 180 deg was precalculated using Mie theory and stored on the computer, given the average diameter and relative refractive index of the polystyrene microspheres at the wavelength. In GPU-MC simulations, the polar angle for each scattering event was obtained by randomly sampling the cumulative distribution function, and the azimuthal angle was randomly chosen from the range of 0 deg to 360 deg. A typical simulation with 10^6 photons was accelerated by more than 30 times using a display card (GTX-650, NVIDIA Corporation, Santa Clara, California) and 16,128 threads, compared to the same simulation on the same computer without using the display card.

2.4 *System Calibration*

Spatially resolved reflectance spectra measured from the four calibration phantoms were used to determine the values of calibration factors $C_1(\lambda)$ and $C_2(\lambda)$ in a calibration formula $R(\lambda) = C_1(\lambda)R_{mea}(\lambda) + C_2(\lambda)$, where $R(\lambda)$ is an expected or calibrated reflectance spectrum and $R_{mea}(\lambda)$ is a measured reflectance spectrum. We used the GPU-MC to calculate the reflectance values of the calibration phantoms for the ROIs described in Sec. 2.1 and twenty-seven wavelengths evenly distributed in the range of 450–700 nm. The scattering coefficients of μ_s and the scattering phase functions were obtained using Mie theory given the concentrations of the microspheres. One set of $C_1(\lambda)$ and $C_2(\lambda)$ was determined for each combination of wavelength and ROIs based on ordinary least-squares estimation. Then, the calibration formula was used to obtain the calibrated spectra $R(\lambda)$ from the measured spectra $R_{mea}(\lambda)$ of a sample under investigation.

After calibration, each set of spatially resolved reflectance spectra was normalized to remove possible fluctuations in detected intensities due to variability in the light source irradiance or in the coupling efficiency at the probe-sample interface. For the perpendicular probe, the calibrated spectra were normalized to the average reflectance of all the ROIs within the wavelength range of 600–700 nm. For the oblique probe, the calibrated spectra were normalized to the average reflectance of the three ROIs along the y axis within the wavelength range of 600–700 nm. We applied normalization in this phantom study to avoid the need for acquiring absolute reflectance measurements that are more difficult to accomplish and may require a specially designed probe.[25] However, it might be advantageous to acquire absolute measurements in future *in vivo* measurements to gain more information about the tissue whose optical properties can vary substantially from site to site, from patient to patient, and with various benign or premalignant conditions.

2.5 *Inverse Model for Extracting Optical Properties of Two-Layered Phantoms*

We estimated the optical properties and top layer thickness of the two-layered phantoms using an iterative curve-fitting approach that minimizes the sum of squared differences between experimental data and Monte Carlo simulated data.[16] Here, the inverse model aimed to fit spectra from all SDSs simultaneously. In other words, only one set of unknown parameters was estimated from each measurement that consisted of four spatially resolved reflectance spectra using the perpendicular probe or six spatially resolved reflectance spectra using the oblique probe. In the inverse model, we applied spectral constraints on $\mu_s'(\lambda)$ and $\mu_a(\lambda)$ to reduce the degree of freedom and improve fitting accuracy. We approximated the $\mu_s'(\lambda)$ of both layers to follow a power law dependence on the wavelength as $A\lambda^{-K}$ in which the parameters A and K of the two layers account for four independent unknown parameters. The $\mu_s(\lambda)$ was then calculated using $\mu_s(\lambda) = \mu_s'(\lambda)/[1\text{-}g(\lambda)]$, where $g(\lambda)$ is

the wavelength-dependent anisotropy factor of the polystyrene microspheres. The $\mu_a(\lambda)$ of the bottom layer was assumed to be $C_{\mathrm{Hb}} \times \varepsilon_{\mathrm{oxyHb}}(\lambda)$ in which C_{Hb} is the unknown hemoglobin concentration and $\varepsilon_{\mathrm{oxyHb}}(\lambda)$, the molar extinction coefficient of oxygenated hemoglobin, was measured in aqueous solutions with a spectrophotometer and used as a known parameter. Finally, the thickness of the top layer D was assumed to be unknown. Therefore, there were six unknown input parameters to be determined.

We used a curve-fitting tool *lsqcurvefit* provided by MATLAB® (MathWorks, Inc., Natick, Massachusetts) to iteratively update the input parameters until convergence. During each iteration of the curve-fitting process, the input parameters were first used to calculate the $\mu_a(\lambda)$ and $\mu_s(\lambda)$ for twenty-seven wavelengths in the range of 450–700 nm. These $\mu_a(\lambda)$ and $\mu_s(\lambda)$ were sent to the GPU-MC to calculate the expected reflectance spectra for the predefined ROIs with either 10^6 (perpendicular probe) or 10^7 (oblique probe) photon packets per wavelength. The simulated spectra were normalized and the weight was adjusted before being compared to the calibrated experimental spectra that were normalized and weight-adjusted in the same way. The purpose of weight-adjusting was to approximately equalize the contribution of each ROI to the squared errors because reflectance intensity monotonically decreases with an increasing SDS. For each set of experimental spectra (i.e., four spectra obtained with the perpendicular probe or six spectra obtained with the oblique probe), we determined ROI-specific multiplicative factors to make the average reflectance of every ROI over the wavelength range of 590–620 nm to be equal. The same set of multiplicative factors was applied to the normalized simulated spectra throughout the iterative curve-fitting process.

To determine the initial values of the six unknown parameters for the iterative curve fitting, we ran GPU-MC simulations with fifty sets of randomly selected parameters and picked the set that generated the least sum of squared differences between the experimental spectra and simulated spectra. The same normalization and weight-adjusting procedure was applied here. The values of the unknown parameters were allowed to change in the ranges of $4800 - 5600\ \mathrm{cm}^{-1}$ (λ expressed in nm), $0.8 \sim 1.2$, $0.5 \sim 3$ g/L, and $0.1 \sim 0.5$ mm for A of both layers, K of both layers, C_{Hb} and D, respectively. We repeated curve fitting of the same set of experimental spectra three times with different initial values for the unknown parameters and chose the set of parameters that yielded the least sum of squared differences to be the recovered parameters of the phantom.

3 Results

3.1 *Calibration of the Spatially Resolved Diffuse Reflectance Spectroscopy System*

We measured calibration phantoms and computed calibration factors for subsequent analysis of all phantom measurements taken on each day. The quality of calibration was evaluated using the coefficient of determination r^2 of the linear regression $R(\lambda) = C_1(\lambda)R_{\mathrm{mea}}(\lambda) + C_2(\lambda)$, described in Sec. 2.4. The r^2 values averaged over all wavelengths and ROIs are about 0.98 for the perpendicular probe and about 0.94 for the oblique probe, indicating highly linear correlation between the measured reflectance and the theoretical reflectance. In order to assess the variability in measurements due to experimental errors or noise, we took repeated measurements without moving the probe on the two-layered phantoms. The results show only 2% deviation in raw spectra measured with the perpendicular probe and 5% deviation with the oblique probe. We also assessed site-to-site variability in reflectance intensity to investigate possible nonuniformity in optical properties of the solid phantoms. The coefficient of variation obtained over five different locations was 2% with the perpendicular probe and 4% with the oblique probe. The results indicate that nonuniformity of the phantoms can be ignored. The spectra averaged over the five measured sites on each phantom were used as the input data to the inverse model.

It is noteworthy that the calibration factors were obtained from aqueous phantoms made of microspheres of two different sizes, which have different scattering phase functions. The high linearity of the calibration results indicates that the DRS system has the same response regardless of the scattering phase function

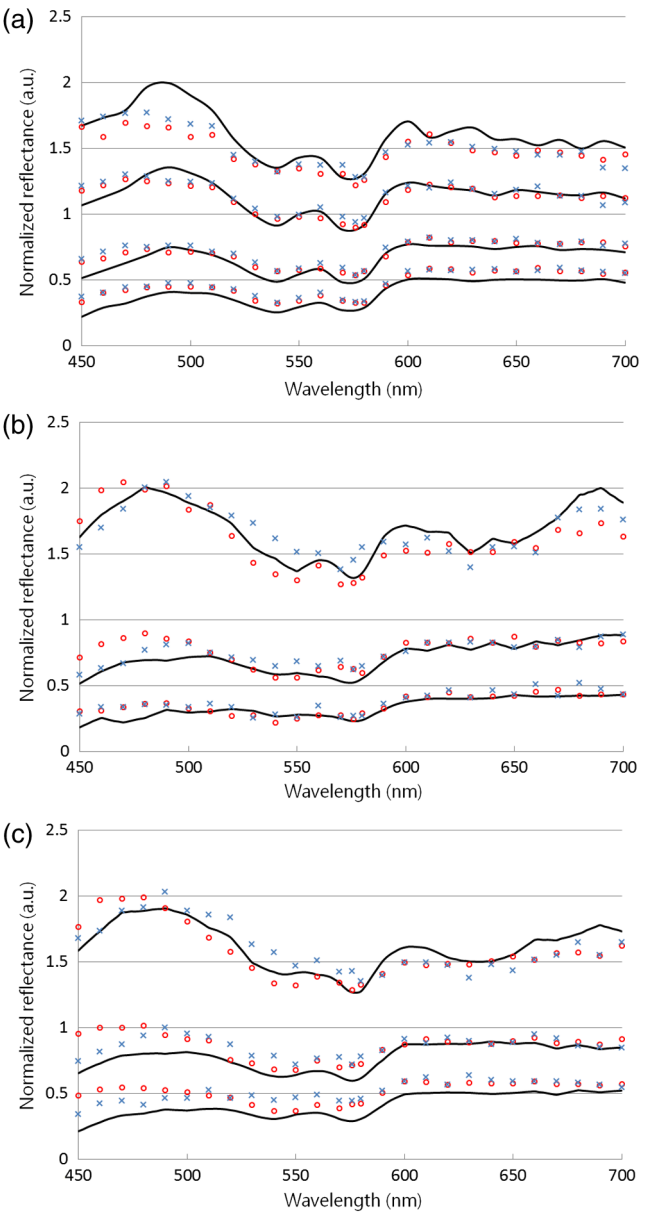

Fig. 2 Comparison of the measured (black solid lines), expected (red circles), and best-fit (blue crosses) spectra of two-layered phantom 6 for (a) the perpendicular probe, (b) ROIs along the *x* axis and (c) ROIs along the *y* axis in the oblique probe. The spectra from top to bottom in each figure correspond to ROIs with an increasing SDS.

of the sample. This is a very important feature to ensure correct calibration of future *in vivo* DRS measurements for quantitative analysis because tissue is expected to have different phase functions from those of the polystyrene microspheres.

3.2 *Extraction of Optical Properties and Top Layer Thickness*

The representative results of two-layered phantom measurements and iterative curve-fitting with the perpendicular and oblique probes are shown in Fig. 2. The expected spectra obtained with the GPU-MC match well with the calibrated experimental spectra, indicating that the model accurately describes the spatially resolved spectra measured with both probes. For a quantitative comparison between the perpendicular and oblique probes, we calculated relative errors of the experimental spectra, taking the expected spectra as the standard, and calculated the root-mean-squared value of the relative errors (rRMSE) over all wavelengths and ROIs used in the GPU-MC. The oblique probe shows a higher discrepancy between the measured and expected spectra (rRMSE = 15%) than the perpendicular probe (rRMSE = 10%). This could be attributed to lower signal-to-noise ratios in the measured spectra as evidenced by a higher deviation between a repeated measurements and to a higher variation in the GPU-MC simulations due to a lack of symmetry and thus a smaller number of photons detected by the oblique probe. On average the rRMSE between the measured and expected spectra of the six two-layered phantoms were 8.4% and 15.5% for the perpendicular and oblique probes, respectively.

Figure 2 also demonstrates a good match between the best-fit spectra and measured spectra for both probes. The rRMSE between the best-fit and measured spectra were 10% and 14% for the perpendicular and oblique probe, respectively. And the overall rRMSE of the six two-layered phantoms were 8.4% and 14.1% for the perpendicular and oblique probe, respectively. The errors of the extracted optical properties and top layer thickness are summarized in Table 2. The errors of $\mu_s'(\lambda)$ are expressed as rRMSE which are calculated over the 27 wavelengths used in the inverse model. The errors of C_{Hb} and D are presented in percentages of the expected values, and absolute values were taken to calculate the mean errors. The errors of the extracted optical coefficients and top layer thickness were mostly less than 30%, and the average errors were no more than 20%. The oblique probe showed higher accuracy in the extracted top layer $\mu_s'(\lambda)$ and higher thickness than perpendicular probe, which is supportive of the enhanced sensitivity to the top layer using the oblique probe geometry as reported in our previous theoretical study.[19] The perpendicular probe showed slightly higher accuracy in the extracted C_{Hb}, which is consistent with the expectation that the perpendicular probe detects photons undergoing longer path lengths in the bottom layer than the oblique probe.

4 Discussion and Conclusions

The accuracy of extracting the unknown parameters of the two-layered phantoms using the two probes is comparable as shown in Table 2. Interestingly, as described in Sec. 3.2, the spectra measured with the oblique probe showed about two times higher rRMSE to the expected spectra than the spectra measured with the perpendicular probe. The curve-fitting results suggest that the oblique probe is more resistant to deviations of experimental spectra from theoretical values. Compared with the perpendicular probe, the oblique probe has more nonoverlapping detection ROIs and therefore provides more information about the spatial distributions of the reflectance, which are characteristics of the absorption and scattering properties of the sample. One of the sources of the larger discrepancy between the expected and measured spectra of the oblique probe is the higher variability in a Monte Carlo simulation of the reflectance collected by the oblique probe due to the lack of symmetry. Experimental errors and noise are minor sources that only contribute about 5% of its variability. We expect that increasing the number of photon packets in GPU-MC simulations during the iterative curve-fitting would improve the accuracy of extracting the optical properties and top layer thickness of two-layered phantoms using the oblique probe.

In the current inverse model, we set the spectra at all SDS to have approximately equal weight when calculating the sum of squared differences between the experimental data and the Monte Carlo simulated spectra. The accuracy of extracting certain unknown parameters could be improved by choosing certain combinations of SDS and wavelength range. For example, selecting a wavelength range of 500–700 nm instead of the original 450–700 nm reduced the errors of the top layer $\mu_s'(\lambda)$ and the bottom layer $\mu_s'(\lambda)$ to 6.5% and 13.4%,

Table 2 rRMSE of $\mu_s'(\lambda)$ and percentage errors of C_{Hb} and D.

Phantom number	Perpendicular probe				Oblique probe			
	Top $\mu_s'(\lambda)$ (%)	Bottom $\mu_s'(\lambda)$ (%)	C_{Hb} (%)	D (%)	Top $\mu_s'(\lambda)$ (%)	Bottom $\mu_s'(\lambda)$ (%)	C_{Hb} (%)	D (%)
1	19	13	15	17	10	21	17	8
2	20	7	1	26	23	27	−10	−14
3	12	28	−3	−21	10	30	10	−4
4	8	8	9	−8	17	10	13	−13
5	12	47	6	−4	9	2	−2	−13
6	31	11	10	−19	4	30	5	−10
Mean	17.1	19.0	7.4	16.0	12.2	20.0	9.4	10.0

respectively, in the case of the oblique probe, and reduced the errors of the top layer $\mu_s'(\lambda)$ and the bottom layer $\mu_s'(\lambda)$ to 14.8% and 17.3% for the perpendicular probe. However, the errors of the extracted C_{Hb} increased slightly to 12.2% and 9% in the cases of the oblique and perpendicular probe, respectively. In this validation study, we did not try to further optimize the fitting results by selecting input data or by adjusting the weights of spectra measured at different SDSs.

The errors shown in Table 2 are expected to be sufficient to detect changes in optical properties associated with premalignant development in the stratified squamous epithelium and underlying stroma. The total hemoglobin concentration extracted from *in vivo* DRS studies has been reported to increase by 50% to 100% in high-grade cervical dysplasia compared to normal cervical tissue.[6,26] The increase in the scattering coefficient of the premalignant epithelium over the normal epithelium has been reported to be about 100% to 200% in the cervix[27] and about 44% in the oral mucosa,[28] both of which were estimated from depth-dependent decays in the reflected intensity of cell nuclei. In addition to providing diagnostic information directly, the $\mu_s'(\lambda)$ and $\mu_a(\lambda)$ extracted from DRS data could be used to remove the influences of scattering and absorption on fluorescence[29] or Raman scattering[30] spectroscopy data obtained with multimodal spectroscopy systems to provide more information for the diagnosis of precancer. For this application, it is desirable to obtain estimates of the optical properties as accurately as possible.

In comparison to a previous study that reported quantification of optical properties of two-layered physical phantoms,[12] our method is able to accurately quantify the unknown top layer thickness and shows higher accuracy in extracted optical coefficients (errors from 7% to 20%). In the previous study, $\mu_a(\lambda)$ and $\mu_s'(\lambda)$ of the two layers were estimated wavelength by wavelength from reflectance values measured at six SDSs; spectral constraints similar to those used in the current study were applied afterward to improve the errors of the estimated $\mu_a(\lambda)$ and $\mu_s'(\lambda)$ from 39–67% to 21–38%. Our approach of simultaneously fitting reflectance spectra measured from multiple ROIs helps to reduce the effect of noise on fitting accuracy[31] and effectively addresses the issue of ambiguity that multiple sets of optical properties generate very similar spatial distributions of reflectance.[11,13]

Another related study extracted μ_a and μ_s' of two-layered liquid phantoms and the thickness of the top layer with the assumptions that the $\mu_s'(\lambda)$ of the two layers is the same and have a fixed scattering power (i.e., the K parameter in this study).[18] The errors of the extracted $\mu_a(\lambda)$ and $\mu_s'(\lambda)$ in the previous study were normalized to the full range used and therefore are not directly comparable to the errors shown in Table 2. The previous study reported the RMSE of the extracted top layer thickness to be approximately constant at 0.1 mm when the thicknesses were in the range of 0–0.45 mm. In the current study, the RMSE of the top layer thickness is about 0.04 mm using the oblique probe. The error of the bottom layer $\mu_a(\lambda)$ reported in the previous study was 20%–100% of the full range for the top layer thickness between 0 and 0.4 mm. The current study achieves a much lower error (10% of the expected value) in the bottom layer $\mu_a(\lambda)$. We suspect that the generally higher accuracy achieved in the current study is due to several factors including running GPU-MC instead of interpolation from a precalculated table every time the input parameters are updated in the curve-fitting process, more accurate modeling of the $\mu_s'(\lambda)$ and scattering phase function, and the use of more detection ROIs. The downside of the inverse model in the current study is computational time: curve-fitting of one spectral dataset takes 1–2 h for the perpendicular probe and about 13 h for the oblique probe. In summary, compared to the methods and results reported by the previous studies, our inverse model not only achieves higher accuracy but also has broader applicability to the detection of changes in tissue optical properties because it does not need to know the top layer thickness[12] and is not limited to tissue with identical $\mu_s'(\lambda)$ in the top and bottom layers.[18]

To extend the methods developed in this study to extracting optical properties of mucosal tissue from *in vivo* DRS measurements, the applicability of the assumptions used in the inverse method needs to be discussed. First, the scattering phase function of polystyrene microspheres is assumed to be known while the phase function of tissue is generally unknown and may vary from one measured site to another. To investigate the effect of mismatched phase functions to the accuracy of the recovered parameters, we also used the HG phase function with a constant anisotropy factor of 0.83 in the GPU-MC for iteratively fitting the spectra measured with the perpendicular probe. Figure 3 shows the representative results comparing the measured, expected, and best-fit spectra of phantom 1. The expected spectra were also calculated with the HG phase function $g = 0.83$. The three sets of spectra agree well with each other, which is similar to the results of using the Mie phase function as shown in Fig. 2(a). The errors of the extracted top layer $\mu_s'(\lambda)$, bottom layer $\mu_s'(\lambda)$, C_{Hb}, and D were 16%, 2%, 18%, and 23%, respectively. The errors are comparable to those shown in Table 2. The results of this investigation suggest an interesting application of the two probes to quantify optical properties of tissue *in vivo*: we could use the data measured with the perpendicular probe to obtain an estimation of the optical properties and top layer thickness of tissue using the HG phase function. Then, because the ranges of the unknown parameters are reduced, we could try to use various phase functions to find the best fit to the data measured with the oblique probe. Scattering phase functions that are obtained with the finite-difference time-domain method[32,33] or the empirical analytical models[34] could provide an initial guess for the tissue scattering phase function.

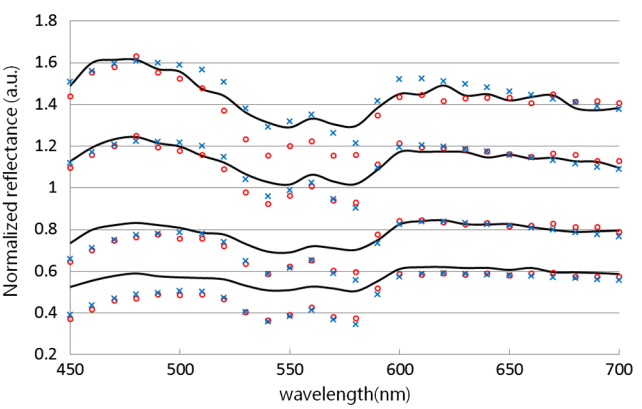

Fig. 3 Comparison of the measured spectra (black solid lines) from phantom 1 using the perpendicular probe to the best-fit spectra using HG phase function in the inverse model (blue crosses) and the expected spectra (red circles) also obtained using HG phase function. The spectra from top to bottom correspond to ROIs with an increasing SDS.

Second, the inverse model requires *a priori* knowledge about the spectral dependences of $\mu_s'(\lambda)$ and $\mu_a(\lambda)$. The power law dependence of $\mu_s'(\lambda)$ on a wavelength has been frequently used to interpret reflectance data from *in vivo* or *ex vivo* tissue measurements. See Ref. 35 for some examples. An additional term of λ^{-4} has been used in some studies to account for the scattering due to refractive index fluctuations much smaller than the wavelength and could be readily added to the model for $\mu_s'(\lambda)$. Although the hemoglobin added to the bottom layer in this study was assumed to be 100% oxygenated, our previous Monte Carlo study considered both oxygenated and deoxygenated hemoglobin concentrations. The errors of the extracted bottom layer $\mu_a(\lambda)$ and oxygen saturation were 6.2% and 7.7% respectively, indicating that the inverse model is capable of accurately quantifying both the oxygenated and deoxygenated hemoglobin concentrations.[19] One additional absorption source or chromophore that might help to improve curve-fitting of the measured reflectance spectra is collagen, whose volume fraction has been estimated to be 15%–20% in the breast[36] and 20%–30% in the skin.[37] To evaluate the effect of including collagen absorption on reflectance intensity, we used optical properties similar to those of the two-layered phantoms and added collagen absorption to the bottom layer $\mu_a(\lambda)$, assuming a 25% volume fraction of collagen and taking the absorption spectrum reported in Ref. 38. The results show a decrease up to 20% in the reflectance intensity in the wavelength range of 460–520 nm. Therefore, it is recommended to include collagen as an absorber in the bottom layer. Other chromophores that might be found in mucosal tissue, such as β-carotene, could also be included in the model since its molar extinction coefficients are known. Including a particular chromophore in the model might help reduce fitting residuals and would need to be verified with further *in vivo* study on mucosal tissue.

The current method will be applied to characterize $\mu_s'(\lambda)$ and $\mu_a(\lambda)$ of the epithelium and the superficial stroma in stratified squamous epithelia *in vivo*. These optical properties are very difficult to measure with conventional methods, such as the integrating sphere and collimated transmission method, due to the challenges associated with removing very thin slices (several hundred microns) of soft tissue for measurements. We will analyze the optical properties of both normal tissue and tissue in various pathological statuses to evaluate the potential of the method for the detection of dysplasia. When more information about the optical properties of the target tissue becomes available, the probe geometry and the efficiency and effectiveness of the inverse model could be further improved.

In conclusion, we report an experimental investigation of a movable DRS instrument with endoscope-compatible probes to recover dysplasia-related optical properties of two-layered tissue phantoms simulating the mucosae that are covered with stratified squamous epithelium. We chose the Monte Carlo method to predict the reflectance detected by the probes because it is accurate and applicable to any illumination and collection arrangement. Polystyrene microspheres and purified human hemoglobin were used to make tissue phantoms whose scattering and absorption properties could be well controlled and theoretically predicted. Accurate calibration of the nonuniform spectral response of the system was indicated by the high linearity ($r^2 \geq 0.94$) of the calibration formula relating the measured reflectance to theoretical values. The results of two-layered phantom experiments demonstrated significant advances in the capability of spatially resolved DRS to simultaneously quantify the $\mu_s'(\lambda)$ and the thickness of the top layer and the $\mu_s'(\lambda)$ and hemoglobin concentration in the bottom layer with errors ranging from 7% to 20%. The oblique probe showed higher accuracy in the extracted top layer $\mu_s'(\lambda)$ and thickness than the perpendicular probe. The developed system and inverse model provide a feasible tool to quantify *in vivo* optical properties of mucosae that are covered with stratified squamous epithelium.

Acknowledgments

We thank the National Science Council (Grant No. #101-2628-E-002-007) in Taiwan and the Molecular Imaging Center of National Taiwan University for financial support of this research. Insightful comments from Dr. Dizem Arifler are highly appreciated.

References

1. J. Q. Brown et al., "Advances in quantitative UV-visible spectroscopy for clinical and pre-clinical application in cancer," *Curr. Opin. Biotechnol.* **20**(1), 119–131 (2009).
2. I. Georgakoudi et al., "Trimodal spectroscopy for the detection and characterization of cervical precancers in vivo," *Am. J. Obstet. Gynecol.* **186**(3), 374–382 (2002).
3. S. McGee et al., "Anatomy-based algorithms for detecting oral cancer using reflectance and fluorescence spectroscopy," *Ann. Otol. Rhinol. Laryngol.* **118**(11), 817–826 (2009).
4. V.T. Chang et al., "Quantitative physiology of the precancerous cervix in vivo through optical spectroscopy," *Neoplasia* **11**(4), 325–332 (2009).
5. A. Amelink et al., "Non-invasive measurement of the microvascular properties of non-dysplastic and dysplastic oral leukoplakias by use of optical spectroscopy," *Oral Oncol.* **47**(12), 1165–1170 (2011).
6. D. Arifler et al., "Spatially resolved reflectance spectroscopy for diagnosis of cervical precancer: Monte Carlo modeling and comparison to clinical measurements," *J. Biomed. Opt.* **11**(6), 064027 (2006).
7. R. Drezek et al., "Light scattering from cervical cells throughout neoplastic progression: influence of nuclear morphology, DNA content, and chromatin texture," *J. Biomed. Opt.* **8**(1), 7–16 (2003).
8. D. Arifler et al., "Light scattering from normal and dysplastic cervical cells at different epithelial depths: Finite-difference time-domain modeling with a perfectly matched layer boundary condition," *J. Biomed. Opt.* **8**(3), 484–494 (2003).
9. J. W. Su, C. Y. Chou, and K. B. Sung, "Three-dimensional refractive index imaging of cells to study light scattering properties of cells and tissue," Chapter 5 in *3-D Reconstruction: Methods, Applications and Challenges*, J. Ashworth and K. Brasher, Eds., pp. 107–123, Nova Science Publishers, Inc., New York (2014).
10. Q. Liu and N. Ramanujam, "Sequential estimation of optical properties of a two-layered epithelial tissue model from depth-resolved ultraviolet-visible diffuse reflectance spectra," *Appl. Opt.* **45**(19), 4776–4790 (2006).
11. Q. Z. Wang, K. Shastri, and T. J. Pfefer, "Experimental and theoretical evaluation of a fiber-optic approach for optical property measurement in layered epithelial tissue," *Appl. Opt.* **49**(28), 5309–5320 (2010).
12. Q. Z. Wang et al., "Broadband ultraviolet-visible optical property measurement in layered turbid media," *Biomed. Opt. Express* **3**(6), 1226–1240 (2012).
13. D. Yudovsky and A. J. Durkin, "Spatial frequency domain spectroscopy of two layer media," *J. Biomed. Opt.* **16**(10), 107005 (2011).
14. D. Yudovsky and L. Pilon, "Rapid and accurate estimation of blood saturation, melanin content, and epidermis thickness from spectral diffuse reflectance," *Appl. Opt.* **49**(10), 1707–1719 (2010).
15. I. Fredriksson, M. Larsson, and T. Stromberg, "Inverse Monte Carlo method in a multilayered tissue model for diffuse reflectance spectroscopy," *J. Biomed. Opt.* **17**(4), 047004 (2012).
16. G. M. Palmer and N. Ramanujam, "Monte Carlo-based inverse model for calculating tissue optical properties. Part I: theory and validation on synthetic phantoms," *Appl. Opt.* **45**(5), 1062–1071 (2006).

17. T. Y. Tseng et al., "Quantification of the optical properties of two-layered turbid media by simultaneously analyzing the spectral and spatial information of steady-state diffuse reflectance spectroscopy," *Biomed. Opt. Express* **2**(4), 901–914 (2011).
18. M. Sharma et al., "Verification of a two-layer inverse Monte Carlo absorption model using multiple source-detector separation diffuse reflectance spectroscopy," *Biomed. Opt. Express* **5**(1), 40–53 (2014).
19. K. B. Sung and H. H. Chen, "Enhancing the sensitivity to scattering coefficient of the epithelium in a two-layered tissue model by oblique optical fibers: Monte Carlo study," *J. Biomed. Opt.* **17**(10), 107003 (2012).
20. H. C. van de Hulst, *Light Scattering by Small Particles*, Dover Publications, Inc., Mineola, New York (1981).
21. S. McGee et al., "Model-based spectroscopic analysis of the oral cavity: impact of anatomy," *J. Biomed. Opt.* **13**(6), 064034 (2008).
22. I. Pavlova et al., "Monte Carlo model to describe depth selective fluorescence spectra of epithelial tissue: applications for diagnosis of oral precancer," *J. Biomed. Opt.* **13**(6), 064012 (2008).
23. A. J. Welch and M. J. C. v Gemert, *Optical-Thermal Response of Laser-Irradiated Tissue*, Plenum Press, New York (1995).
24. D. Arifler et al., "Reflectance spectroscopy for diagnosis of epithelial precancer: model-based analysis of fiber-optic probe designs to resolve spectral information from epithelium and stroma," *Appl. Opt.* **44**(20), 4291–4305 (2005).
25. B. Yu, H. L. Fu, and N. Ramanujam, "Instrument independent diffuse reflectance spectroscopy," *J. Biomed. Opt.* **16**(1), 011010 (2011).
26. V.T.C. Chang et al., "Visible light optical spectroscopy is sensitive to neovascularization in the dysplastic cervix," *J. Biomed. Opt.* **15**(5), 057006 (2010).
27. T. Collier et al., "Real-time reflectance confocal microscopy: comparison of two-dimensional images and three-dimensional image stacks for detection of cervical precancer," *J. Biomed. Opt.* **12**(2), 024021 (2007).
28. A. L. Clark et al., "Detection and diagnosis of oral neoplasia with an optical coherence microscope," *J. Biomed. Opt.* **9**(6), 1271–1280 (2004).
29. G. M. Palmer and N. Ramanujam, "Monte-Carlo-based model for the extraction of intrinsic fluorescence from turbid media," *J. Biomed. Opt.* **13**(2), 024017 (2008).
30. C. Reble et al., "Quantitative Raman spectroscopy in turbid media," *J. Biomed. Opt.* **15**(3), 037016 (2010).
31. R.M.P. Doornbos et al., "The determination of in vivo human tissue optical properties and absolute chromophore concentrations using spatially resolved steady-state diffuse reflectance spectroscopy," *Phys. Med. Biol.* **44**(4), 967–981 (1999).
32. C. Kortun, Y. R. Hijazi, and D. Arifler, "Combined Monte Carlo and finite-difference time-domain modeling for biophotonic analysis: implications on reflectance-based diagnosis of epithelial precancer," *J. Biomed. Opt.* **13**(3), 034014 (2008).
33. W. C. Hsu et al., "Investigating the backscattering characteristics of individual normal and cancerous cells based on experimentally determined three-dimensional refractive index distributions," *Proc. SPIE* **8553**, 85531O (2012).
34. J. D. Rogers, I. R. Capoglu, and V. Backman, "Nonscalar elastic light scattering from continuous random media in the Born approximation," *Opt. Lett.* **34**(12), 1891–1893 (2009).
35. S. L. Jacques, "Optical properties of biological tissues: a review," *Phys. Med. Biol.* **58**(11), R37–61 (2013).
36. R. Nachabe et al., "Diagnosis of breast cancer using diffuse optical spectroscopy from 500 to 1600 nm: comparison of classification methods," *J. Biomed. Opt.* **16**(8), 087010 (2011).
37. S. H. Tseng et al., "Noninvasive evaluation of collagen and hemoglobin contents and scattering property of in vivo keloid scars and normal skin using diffuse reflectance spectroscopy: pilot study," *J. Biomed. Opt.* **17**(7), 077005 (2012).
38. A. S. Nunez, "A physical model of human skin and its application for search and rescue," Ph.D. Thesis, Air Force Institute of Technology (2009).

Kung-Bin Sung received his MS and PhD degrees in biomedical engineering from the University of Texas at Austin in 1999 and 2003, respectively. He worked as a research scientist in Intel Corporation between 2003 and 2006. He joined the Department of Electrical Engineering and Graduate Institute of Biomedical Electronics and Bioinformatics at National Taiwan University in 2006. His research focuses on developing optical spectroscopy and microscopy techniques for early diagnosis of cancer and precancer.

Kuang-Wei Shih received his MS degree from the Graduate Institute of Biomedical Electronics and Bioinformatics, National Taiwan University in 2013. His main contribution to this work was the assembly and validation of a movable reflectance spectroscopy system.

Fang-Wei Hsu is currently a graduate student majoring in biomedical electronics in the National Taiwan University. Her research is focused on simulating spectra by the Monte Carlo algorithm and developing quantitative optical spectroscopy techniques.

Hong-Po Hsieh received his BS degree in electrical engineering in 2012 from theNational Taiwan University. He is currently a MS student in the Graduate Institute of Biomedical Electronics and Bioinformatics, National Taiwan University. The majority of his work in this group is data analysis.

Min-Jie Chuang is a MS student at the Graduate Institute of Biomedical Electronics and Bioinformatics, National Taiwan University. His research focuses on the development of diffuse reflectance spectroscopy and fluorescence spectroscopy for early cancer diagnosis.

Yi-Hsien Hsiao is currently a MS student at the Graduate Institute of Biomedical Electronics and Bioinformatics, National Taiwan University. Her research focuses on the development of diffuse reflectance spectroscopy and fluorescence spectroscopy for early cancer diagnosis.

Yu-Hui Su received her MS degree from the Graduate Institute of Biomedical Electronics and Bioinformatics, National Taiwan University in 2013. Her main contribution to this work was the construction of tissue phantoms and analysis of spectral data.

Gen-Hao Tien is currently an MS student at the Graduate Institute of Biomedical Electronics and Bioinformatics, National Taiwan University. His research focuses on designing systems of diffuse reflectance spectroscopy and fluorescence spectroscopy and using the Monte Carlo simulation method to quantify the optical properties of tissue for early cancer diagnosis.